



Shahrood University of
Technology



Iranian Society of
Mining Engineering
(IRSME)

PFC Simulation of Brazilian Tensile Strength Test in Geomaterials' Specimens with T-shaped Non-persistent Joints

Vahab Sarfarazi¹, Hadi Haeri², Fereshteh Bagheri¹, Erfan Zarrin ghalam¹, and Mohammad Fatehi Marji^{3*}

1. Department of mining engineering, Hamedan University of technology, Hamedan, Iran

2. Department of Mining Engineering, Higher Education Complex of Zarand, Zarand, Iran

3. Department of Mine Exploitation Engineering, Faculty of Mining and metallurgy, Institute of Engineering, Yazd University, Yazd, Iran

Article Info

Received 14 November 2022

Received in Revised form 21
November 2022

Accepted 4 December 2022

Published online 4 December
2022

DOI: 10.22044/jme.2022.12418.2252

Keywords

T-shaped non-persistent joint

Joint angle

Joint length

PFC2D

Abstract

The tensile strengths of geomaterials such as rocks, ceramics, concretes, gypsum, and mortars are obtained based on the direct and indirect tensile strength tests. In this research work, the Brazilian tensile strength tests are used to study the effects of length and inclination angle of T-shaped non-persistent joints on the mechanical and tensile behaviors of the geomaterial specimens prepared from concrete. These specimens have a thickness of 40 mm and a diameter of 100 mm, and are prepared in the laboratory. Two T-shaped non-persistent joints are made within each Brazilian disc specimen. The Brazilian disc specimens with T-shaped non-persistent joints are tested experimentally in the laboratory under axial compression. Then these tests are simulated in the two-dimensional particle flow code (PFC2D) considering various notch lengths of 6, 4, 3, 2, and 1 cm. However, different notch inclination angles of 0, 30, 60, 90, 120, and 150 degrees are also considered. In this research work, 12 specimens with different configurations are provided for the experimental tests, and 18 PFC2D models are made for the numerical studies of these tests. The loading rate is 0.016 mm/s. The results obtained from these experiments and their simulated models are compared, and it is concluded that the mechanical behavior and failure process of these geomaterial specimens are mainly governed by the inclination angles and lengths of the T-shape non-persistent joints presented in the samples. The fracture mechanism and failure behavior of the specimens are governed by the discontinuities, and the number of induced cracks when the joint inclination angles and joint lengths are increased. For larger joints when the inclination angle of the T-shaped non-persistent joint is around 60 degrees, the tensile strength is minimum but as it is closed to 90 degrees, the compressive strengths are maximum. However, an increase in the notch length increase the overall tensile strength of the specimens. The strength of samples decreases by increasing the joint length. The strain at the failure point decreases by increasing the joint length. It is also observed that the strength and failure process of the two sets of specimens and the corresponding numerical simulations are consistence.

1. Introduction

Natural rock masses consist of the main structure of the surface and underground geo-mechanical projects used in many engineering fields such as mining, petroleum, civil,

geological, and environments [1]. The discontinuities in form of joints, flaws, and fractures may exist in most of the rock masses, which alter the mechanical behavior of the rock

✉ Corresponding author: mohammad.fatehi@gmail.com (M. Fatehi Marji)

structure under various *in situ* loading conditions [2]. Some discontinuities such as joints occur naturally in parallel or regularly spaced sets of discontinuities in rock masses. These geometrical sets may have different orientations, which produce natural rock blocks in the rock mass. Many researchers usually considered the effects of one or two discontinuities on the mechanical characteristics of rock specimens in the laboratory [3-14]. It is very difficult to prepare specimens of natural rocks with discontinuities. Therefore, the specimens of rock-like materials containing artificial joints are used in laboratories for studying the physical and mechanical characteristics of geo-materials [15-29]. Several researchers [5-7, 15] used cutting machines with a water jet of high pressure to produce the required cracks in granite and sandstone samples. Most of the previous studies are focused on the behavior, strength, and fracture mechanics of geo-materials under various environments. The fracture mechanics of geo-material samples considering the initiation, propagation, and coalescence of one, two, and three cracks in the specimen can be studied and understood [18]. However, the discontinuities in the geo-materials such as rocks and concrete mostly occur in a set form, for example, as one or two or more joint sets in rock masses. Many investigators worked on the effects of discontinuities such as faults and joint sets with different orientations and geometry on the stability and ground subsidence of huge underground structures such as tunnels and mines which pass through rock masses [30]. Therefore, considering the effects of multiple joint sets and cracks with different orientations on the strength and mechanical characteristics of the geo-materials are of paramount importance in the design of underground rock structures [31-34]. Most of these investigations worked on the failure and fracture mechanisms in rock masses with multiple cracks and joints considering various geometries and loading environments. The crack patterns, propagations, and coalescences in various geo-material specimens were studied. These investigations claimed that the fracture patterns and failure mechanisms in these specimens were very close to the results obtained by considering only two cracks or joints with different orientations in the geo-material specimens [35]. They also stated that the rock

strengths and structural failures mainly depend on the principal stresses and joints' geometries and joints' conditions [35]. Many experimental tests on the subject used laboratory rock-like material specimens to model the jointed rocks. However, rock-like material specimens with multiple joints and flaws can be fabricated in the laboratory for studying the effects of joint sets and their orientations on the mechanical behavior of natural rock masses [35]. The numerical simulations of these laboratory tests are adopted by many investigators to consider the influences of various cracks and joint patterns on the fracture mechanisms and failure modes of jointed rock masses. The various scenarios and complexity of these geo-mechanical problems can be modeled by the sophisticated numerical methods such as finite element methods like RFPA2D and RFPA3D used by Tang *et al.* [37] and Wang *et al.* [38], respectively, boundary element method (displacement discontinuity method used by Fatehi Marji [39], extended finite element method used by Xie *et al.* [40] and discrete element method used by Cheng *et al.* [34]. The crack coalescences phenomena in the specimens of red sunstone with two random flaws under compression were simulated in PFC2D by Yang *et al.* [15]. The effects of two original random cracks in the specimens of red sandstones on the stresses are investigated, and the mechanisms of cracks' coalescences under uniaxial compression are studied in the recent years. However, the crack analyses considering the initiations, extensions, and coalescences of natural fractures in the jointed rock masses embedding the tunnels, and underground openings have been investigated by the researchers [41-44]. In the previous research work, the effect of two parallel notches on the failure behavior of a notched sample has been investigated. In this work, the effect of the un-parallel notch on the tensile behavior of rock-like sample has been investigated. The experimental tests and the discrete element simulation technic are used to study the effects of crack inclination angles and lengths of the non-persistent joints with T shapes on the Brazilian tensile strength of the rock bridges in between the joints in the rock mass.

2. Uniaxial Compression Test for Rock-like Specimens with Non-persistent T-shaped Joint

The uniaxial compression and Brazilian tensile tests on the rock-like specimens are used for experimental tests and their numerical simulation. In this experiment, the jointed rock mass is physically modeled by the specimens of rock-like materials in the laboratory. As shown in Figure 1, the specimens are prepared from cement

and water with a mass ratio of 2:1, respectively. The sample size (diameter * thickness) was 12 cm * 4 cm. Open cracks are established with the insertion of metal sheets in the material past before casing and pulling them out after the solidification of the specimen.

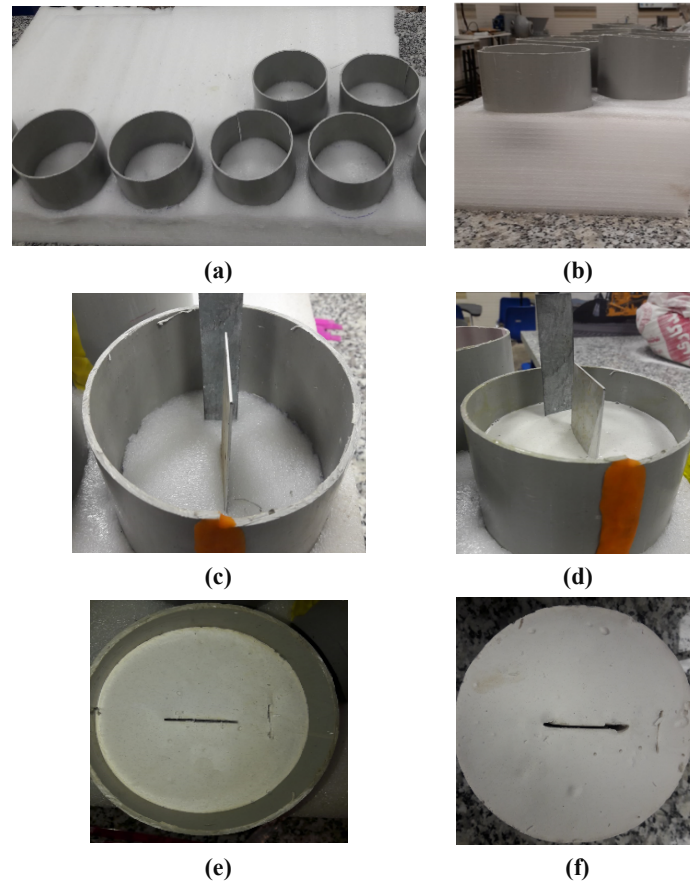


Figure 1. a) Frame with diameter of 10 cm and thickness of 40 cm. b) Frame with diameter of 10 cm and thickness of 40 cm. c) Shim with dimension of 100 mm × 1 mm × 60 mm inside the plastic fiber. e) Plaster slurry inside the mold e) Aluminum sheet is removed from the mold. f) Sample consisting of T-shaped non-persistent joint.

These experimental samples are prepared in several sets for accomplishing various tests in the laboratory. T-shaped non-persistent cracks were formed in the model. The open cracks with various dip and inclination angles are located in various experimental samples. The small prefabricated cracks in this experiment are 1 cm, 2 cm, and 3 cm (Figure 2a). The large prefabricated cracks are 6 cm, 4 cm, and 2 cm (Figure 2b). The opening of the notch is 1 mm. The specimen sets are kept in a cool and dry laboratory room for 28 days. The angle of joint

with larger length related to the horizontal axis was 0 (Figures 3a, 4a, and 5a), 30 (Figures 3b, 4b, and 5b), 60 (Figures 3c, 4c, and 5c), 90 (Figures 3d, 4d, and 5d). The angle between the large joint and the small joint was 90 degrees (Figures 3-5). 12 types of T-shaped non-persistent joints were used in this experiment. The crack arrangement and specimen number of each specimen were depicted in Figures 3-5. The non-persistent joints of the T-shape are located within the specimens, and the Brazilian tensile strength tests are carried out with the electrohydraulic universal testing

machine in the laboratory. The electrohydraulic universal testing machine was used to perform the Brazilian test for the non-persistent joints. The experimental system includes the loading

control system, testbed, and data acquisition system. These experiments are performed at a loading rate of 0.005 mm/s, as shown in Figure 6.

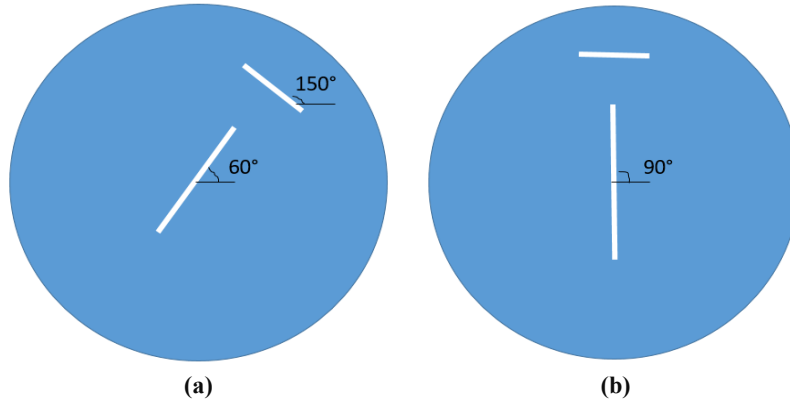


Figure 2. Two T-shaped joints with large joint angle of a) 0, b) 30, c) 60, d) 90.

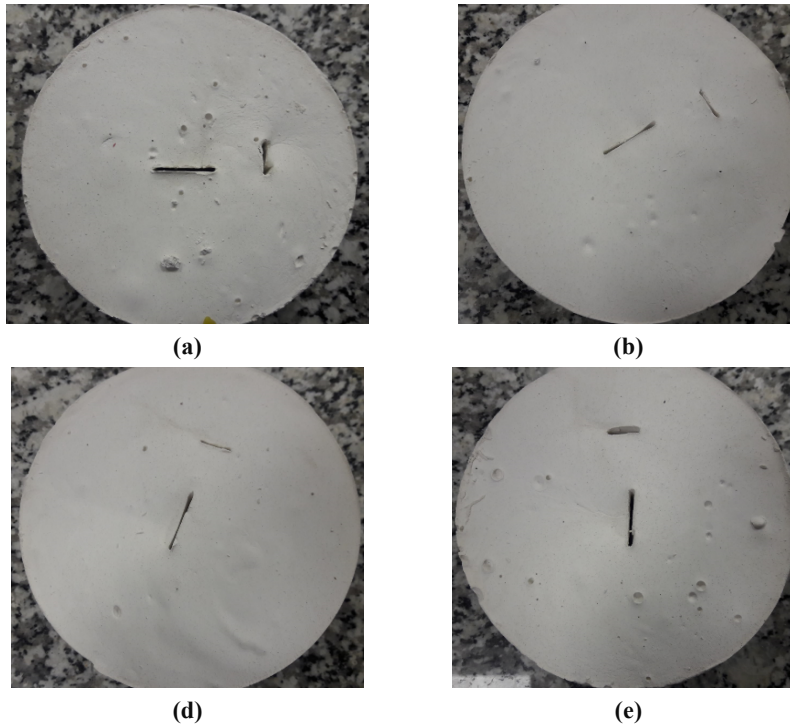


Figure 3. T-shaped joint with large joint angle of a) 0, b) 30, c) 60, d) 90; large joint length was 2 cm.

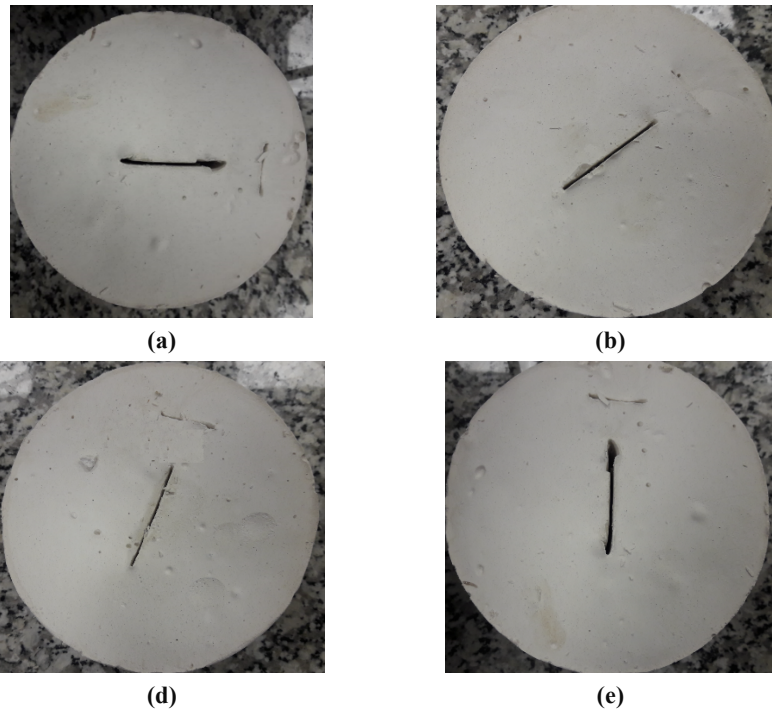


Figure 4. T-shaped joint with large joint angle of a) 0, b) 30, c) 60, d) 90; large joint length was 4 cm.

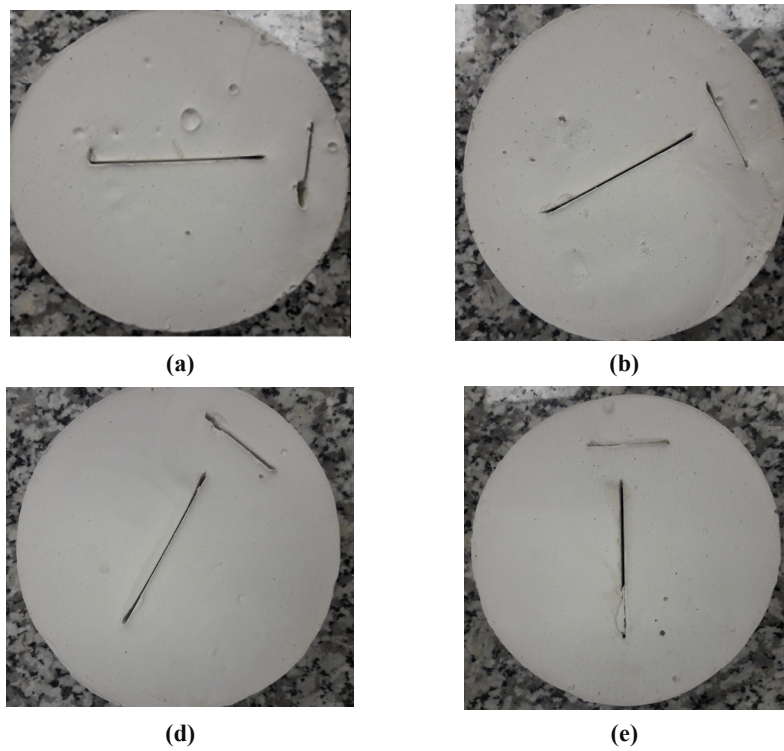


Figure 5. T-shaped joint with large joint angle of a) 0, b) 30, c) 60, d) 90; large joint length was 6 cm.



Figure 6. Specimens are placed between plates of the loading machine.

3. Failure Process Observed in Laboratory Tests

The failure process in the experimental tests of the rock-like specimens with T-shaped non-persistent joints are studied considering various joints of different lengths and inclination angles.

3.1. Large joint is 2 cm and small joint is 1 cm

The failure mechanism and fracturing pattern in the specimens with non-persistent joints of 2 cm and 1 cm in length are shown in Figure 7. Various joint angles are considered, and the initiation and growth patterns of the induced cracks are shown. Figure 7a shows the initiation mechanism of two tensile cracks starting from the tips of the large crack when its inclination angle is below 30 degrees. Figure 7b and Figure 7c show the failure mechanism of the specimens when the crack

inclination angles are 30 and 60 degrees, respectively. The large crack starts its propagation path from the tips but induced tensile cracks may initiate from the middle part (wall) of the small cracks as the inclination angle increases. Figure 7d shows the crack growing path for the specimens of large cracks with a 90-degree inclination angle. The tensile cracks initiate from the tips of the large crack, and continue their path toward the specimen's boundary in the direction of the applied load. The tensile cracks may also initiate from the tip, and the middle part of the small crack and propagate within the specimen till coalescence with the other cracks or meet the specimen's boundary. Tensile cracks surfaces are smooth without pulverized material. Any characteristics of shear displacement are not observed in failure surface.

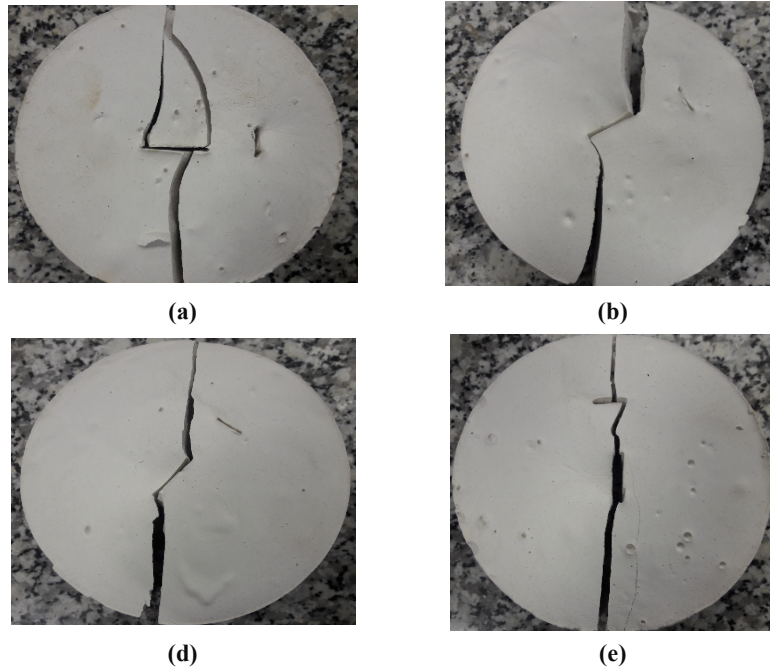


Figure 7. Failure mechanisms of rock-like material specimens with two non-persistent joints when the inclination angle of large crack is a) 0, b) 30, c) 60, d) 90.

3.2. Small joint is 2 cm and large joint 4 cm

The failure and fracturing process in the rock-material specimens with two non-persistent joints are shown in Figure 8. As shown in Figure 8a for the case of a large crack with 0 inclination angle concerning the loading direction, two induced tensile cracks are initiated from the large crack and propagated in the loading direction till reach to the specimen's boundaries. In this case, one tensile crack may also get initiated from the middle of the small crack and extend to the lower boundary of the specimen. For the case of 30 degrees inclination angle for a large joint as shown in Figure 8b, a tensile crack may be

induced from the upper tip of the large joint and extend up in the direction of loading and meet the boundary of the specimen. For the inclination angles 60 and 90 degrees of the large crack, the tensile crack may be initiated from the lower tip of the bigger crack and extend toward the boundary as shown in Figures 8c and 8d. For the higher inclination angles of a large crack, a tensile crack may be initiated from the wall of the small joint and extend toward the specimen's boundary. Inspection of the failure surface shows that there is not any pulverized material in the failure surface, and also failure surface was slickenside, which means that the dominant mode of failure was tensile.

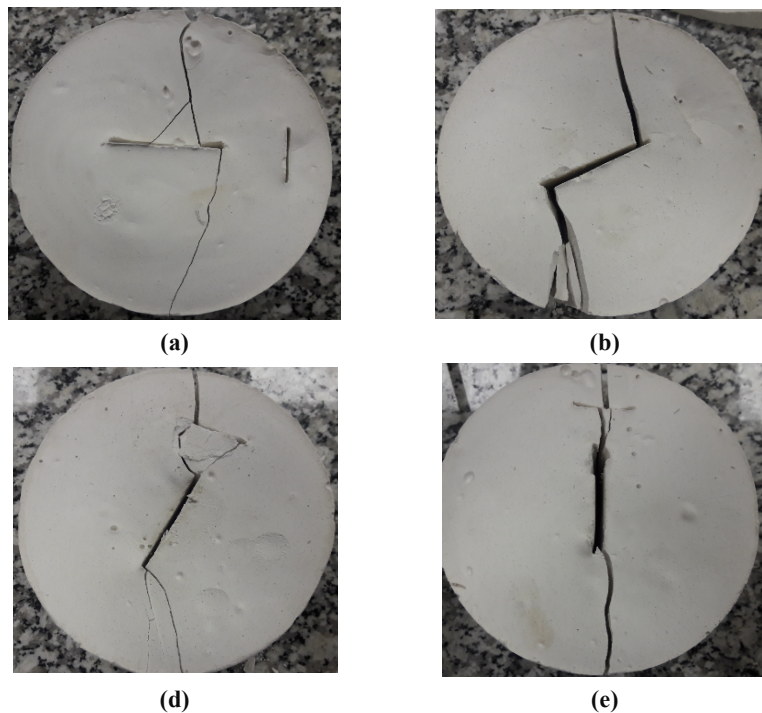


Figure 8. Failure pattern of specimens containing two non-persistent joint with large joint angle of a) 0, b) 30, c) 60, d) 90.

3.3. Large joint length was 6 cm and small joint length was 3 cm

The two non-persistent joints existing in the rock-like material specimens modeled in PFC and the specimen's failure process is shown in Figures 9a to 9d considering the changes in the inclination angle of the large crack concerning the applied loading direction. In these analyses, the inclination angle of the large crack changes from 0 to 90 degrees with an interval of 30 degrees. Figure 9a shows that the failure process for the case that the large crack angle is 0 degrees. In this case, two wing cracks are initiated from the two tips of the large crack, and one tensile crack is initiated from the middle part. These tensile cracks are propagated toward the specimen's boundaries. Figures 9b and 9c show

the failure process of the specimens for the cases of 30 and 60 degrees inclination angles of the large crack, respectively. In either of these cases, two wing cracks are initiated from the upper and lower tips of the large crack and propagate toward the respective specimens' boundaries in the direction of the applied load. For the case of 90 degrees inclination angle of a large joint, two tensile cracks are initiated from the upper and lower tips of the crack and propagate toward the respected boundaries parallel to the loading direction as shown in Figure 9d. In these cases, the fracture surfaces are clean and slickenside with no pulverized material in between. This feature demonstrates the domination of mode I fracture in the specimens during the failure process.

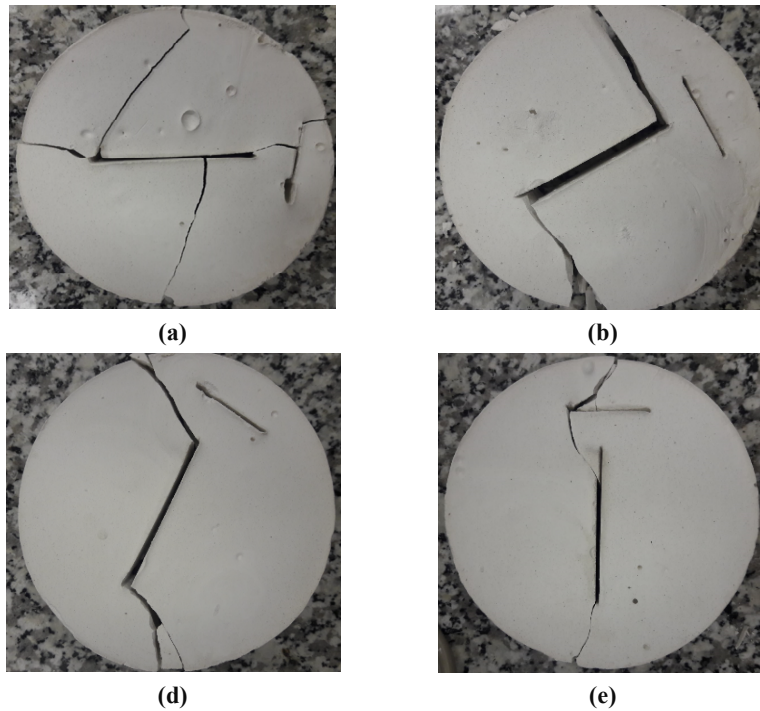


Figure 9. Mechanism of failure process in the rock-like material specimens containing two non-persistent joints with large and small sizes; the large joint inclination angle changes as a) 0, b) 30, c) 60, d) 90 degrees, respectively.

3.4. Specimens' strength affected by joint inclination angle

The strengths of modeled specimens are affected by the inclination angles of joints, and their lengths as shown in Figure 10. The strength

of the specimens is maximum for right angle large joints and minimum for 60 degrees inclination angle. On the other hand, as the joints' lengths increase, strengths of the samples decrease.

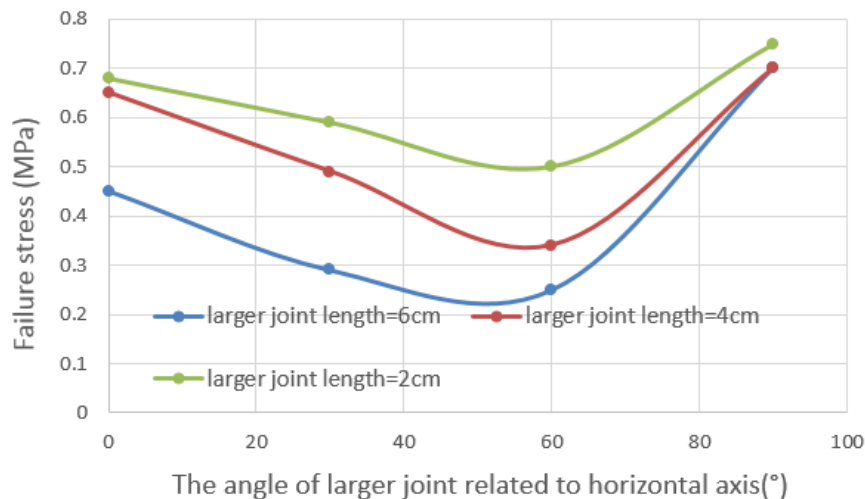


Figure 10. Effects of joint length and joint inclination angle on strength of the modelled specimen.

4. Numerically Simulated Tests

4.1. Two dimensional particle flow code

The discrete element analysis of geo-mechanical problems in two dimensions can be accomplished using the particle flow code (PFC2D). The geo-material specimens are considered as an assembly of circular particles, and the explicit time-step finite difference algorithm is established in PFC2D based on the force-displacement relations obeying the second law of Newton [45]. The contact bond and parallel bond models are adopted in the discrete element code. In the contact bond models, only force and displacement are modeled at the contact points with no resistance to momentum. On the other hand, in the parallel bond, the areas of glue and contacts are considered in a parallel line form, which can resist both forces and moments. Therefore, the joints' contact surfaces can be easily simulated by the parallel bond model scheme. Potyondy and Cundall (2004) proposed the parallel bond model for simulating the contact points and surfaces in the geo-material samples such as rock specimens. In the failure process of the geo-material specimens, the contact forces induce the stresses in the particle assembly so that

the bonds break and form micro-cracks, where the induced local stresses exceed the strength of the parallel bonds in the geo-materials.

4.2 Preparation and calibration of PFC2D model for rock-like material

In this work, PFC2D models of the specimens are generated in form of particle assemblies as described by Potyondy and Cundall [45]. The standard procedure includes generating particle assembly, implementing the isotropic stress state, packing the particles in the assembly, eliminating the floating particles from the assembly, and installing the bonds in between the packed particles. In this modeling techniques, the gravity effects of the particles are neglected because the stress gradient induced due to gravity may not affect the macroscopic behavior of the modeled specimen. However, for calibrating the PFC2D models, the Brazilian tensile strength and the uniaxial compressive strength tests were carried out in the laboratory [2]. The micro-parameters used for the model tests are calibrated by adopting the standard trial and error algorithm suggested by Potyondy and Cundall [45]. These adjusted micro-parameters are listed in Table 2.

Table 2. Micro properties used to represent intact rock.

Parameter	Value	Parameter	Value
Type of particle	Disc	Parallel-bond radius multiplier	1
Density (kg/m ³)	3000	Young's modulus of parallel bond (GPa)	4
Minimum radius (mm)	0.27	Parallel bond stiffness ratio	1.7
Size ratio	1.56	Particle friction coefficient	0.4
Porosity ratio	0.08	Parallel bond normal strength, mean (MPa)	15
Damping coefficient	0.7	Parallel bond normal strength, SD (MPa)	1.5
Contact Young's modulus (GPa)	4	Parallel bond shear strength, mean (MPa)	15
Stiffness ratio	1.7	Parallel bond shear strength, SD (MPa)	1.5

Figures 11a and 11b show the experimental uniaxial compression test and numerical simulation, respectively. Figures 11c and 11d show the experimental Brazilian test and numerical simulation, respectively. The results show a well-match between the experimental test

and numerical simulation. Also the obtained specimen properties from the numerical models such as elastic modulus, Poisson's ratio, and UCS values agree well with the experimental values, as indicated in Table 3.

Table 3. Comparison of macro-mechanical properties between experiments and model.

Mechanical properties	Experimental results	PFC2D model results
Elastic modulus (GPa)	9	9.2
Poisson's ratio	0.18	0.19
UCS (MPa)	15	15
Brazilian tensile strength (MPa)	1	1.2

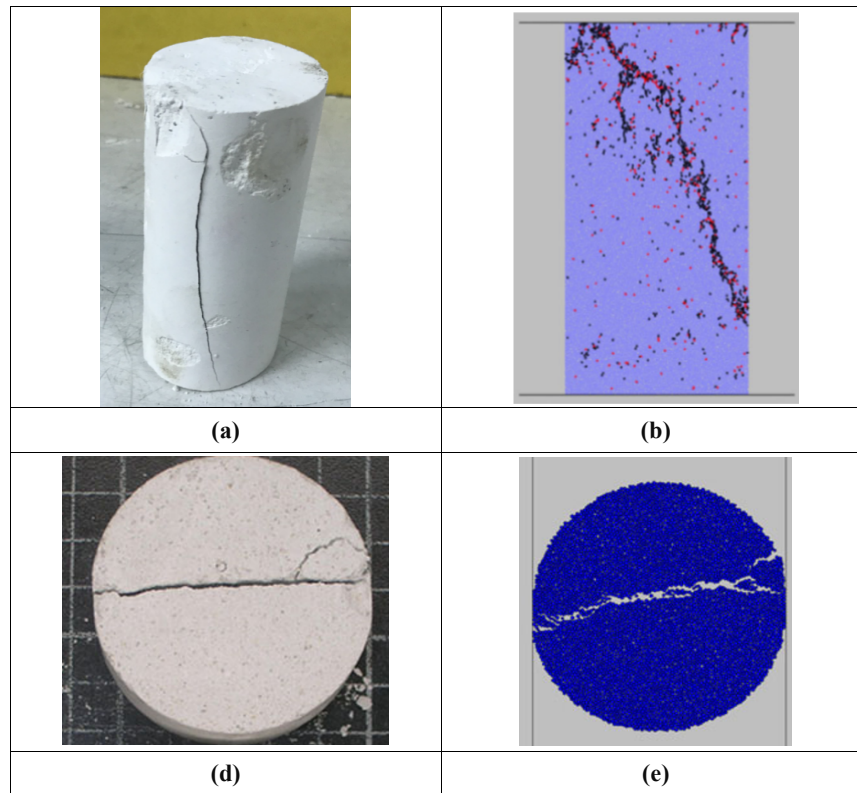


Figure 11. a) Experimental compression test, b) numerical compression test, c) experimental Brazilian test, and d) numerical Brazilian test.

4.3 Numerical compressive tests on non-persistent open joint

The Brazilian disc specimens containing joints are simulated in PFC2D using the calibrated data already determined in the previous section. Figures 12, 13, and 14 show the PFC-modelled specimens. The diameter of the modeled particle assembly is 100 mm, and 12878 discs of a minimum 0.27 mm radius are used to model the circular disc specimen. Figures 12 to 14 also show the non-persistent joints in the assembly and the two walls surrounding the whole model. In this research work, the non-persistent joints have T-shapes and two pre-fabricated joints are considered, one is the small joint, and another one is the large joint. The small joint is about 10 mm in length and 1 mm in width, as shown in Figure 12. The 20 mm and 30 mm cracks are shown in

Figures 13 and 14, respectively. On the other hand, the length of the large crack is 20 mm in Figure 12, 40 mm in Figure 13, and 60 mm in Figure 14. The inclination angle of the larger joint concerning the horizontal axis is zero in Figures 12a, 13a, and 14a. This angle is 30 degrees in Figures 12b, 13b, and 14b; 60 degrees in Figures 12c, 13c, and 14c; and 90 degrees in Figures 12d, 13d, and 14d. The two small and large non-persistent joints are at right angles to each other in form of a T. In this modeling procedure, 12 types of T-shaped joints are used and arranged. The modeled specimens are depicted in Figures 12, 13, and 14. The applied uniaxial force is exerted on the specimens through the upper and lower walls, and the uniaxial stress is recorded from the reaction forces of the specimen's upper wall.

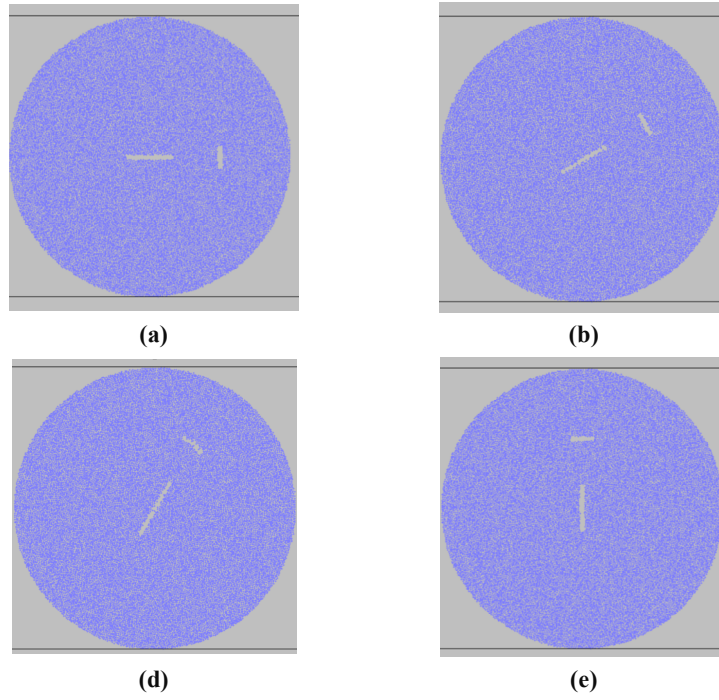


Figure 12. T-shaped joint with large joint angle of a) 0, b) 30, c) 60, d) 90, e) 120, and f) 150.

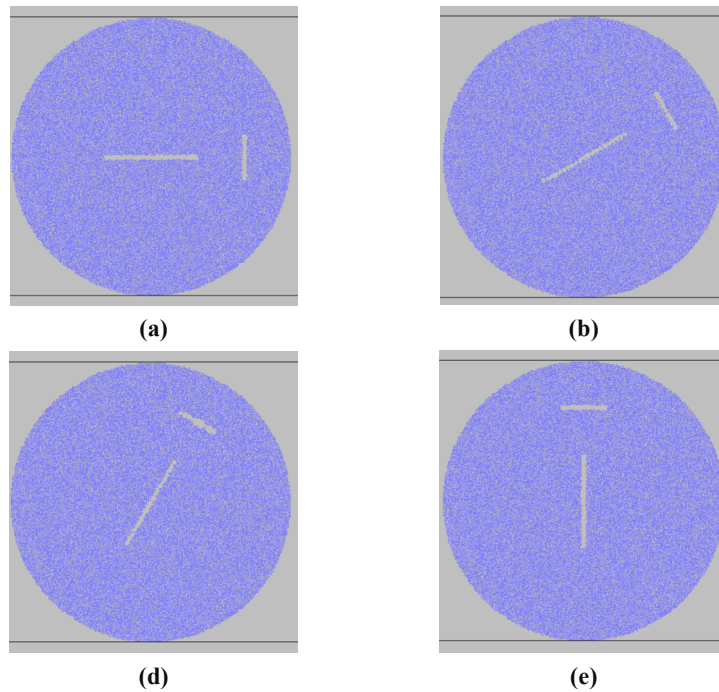


Figure 13. T-shaped joint with large joint angle of a) 0, b) 30, c) 60, d) 90, e) 120, and f) 150.

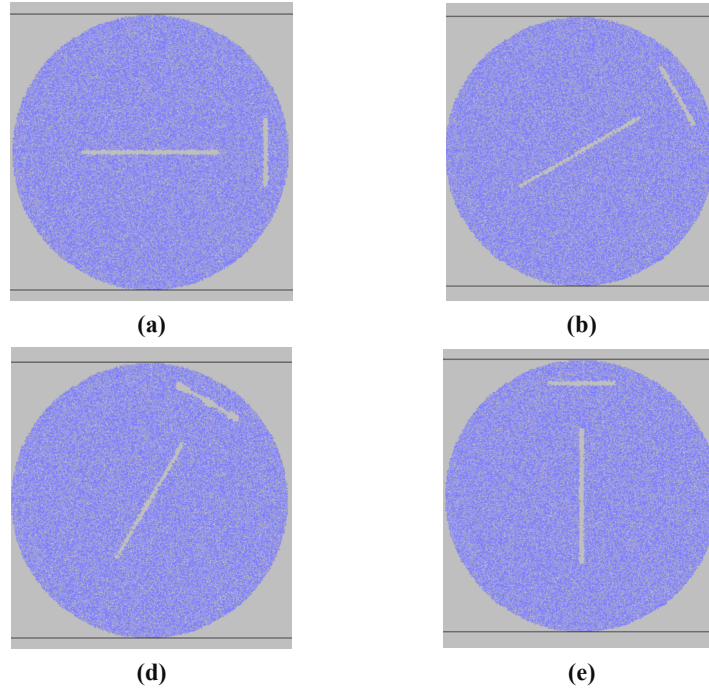


Figure 14. Two T-shaped joints with large joint angle of a) 0, b) 30, c) 60, d) 90, e) 120, and f) 150.

4.4. Effects of joint configuration on the failure behavior of modelled samples

a) Large joint length was 2 cm and small joint length was 1 cm

The failure process in the modeled specimens with the two non-persistent joints is shown in

Figure 15. The tensile cracks are shown in black color, and the shear ones are depicted in red color. The stress and strain curves for the four models of 0, 30, 60, and 90 joint angles are shown in Figure 16.

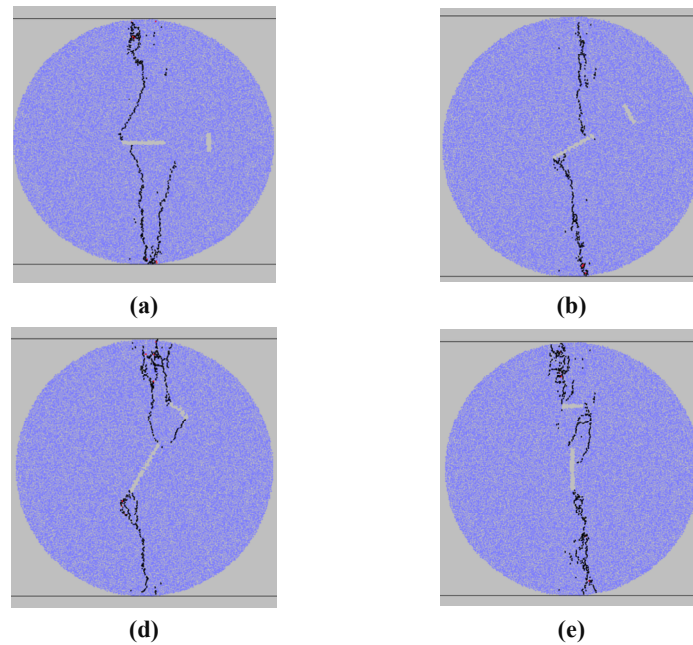


Figure 15. Failure pattern of specimens containing three non-persistent joint with large joint angle of a) 0, b) 30, c) 60, d) 90, e) 120, and f) 150.

In the specimens with a horizontal large joint angle, the initiated tensile cracks from the upper and lower tips are shown in Figure 15a. These tensile cracks are propagated in the direction of the applied load toward the boundary of the specimen. Another tensile crack is initiated from the middle part of the large crack and propagated toward the lower boundary of the specimen. Figure 15b shows the failure process in the modeled specimens with a large joint of 30 degrees. The two tensile cracks were initiated from the upper and lower tips of the large cracks and propagated in the applied loading direction

toward the respected boundaries of the specimen. Figures 15c and 15d show the failure process in the modeled specimens with the joints of 60 and 90 degrees joint angles, respectively. In these two cases, the tensile cracks are initiated from the upper and lower tips of the large crack. One tensile crack is also initiated from the middle part of the large crack and extended in the direction of loading toward the lower boundary of the modeled specimen. The stress-strain curves shown in Figures 16 demonstrates the mechanical behavior of the models with different inclination angles for the larger joint.

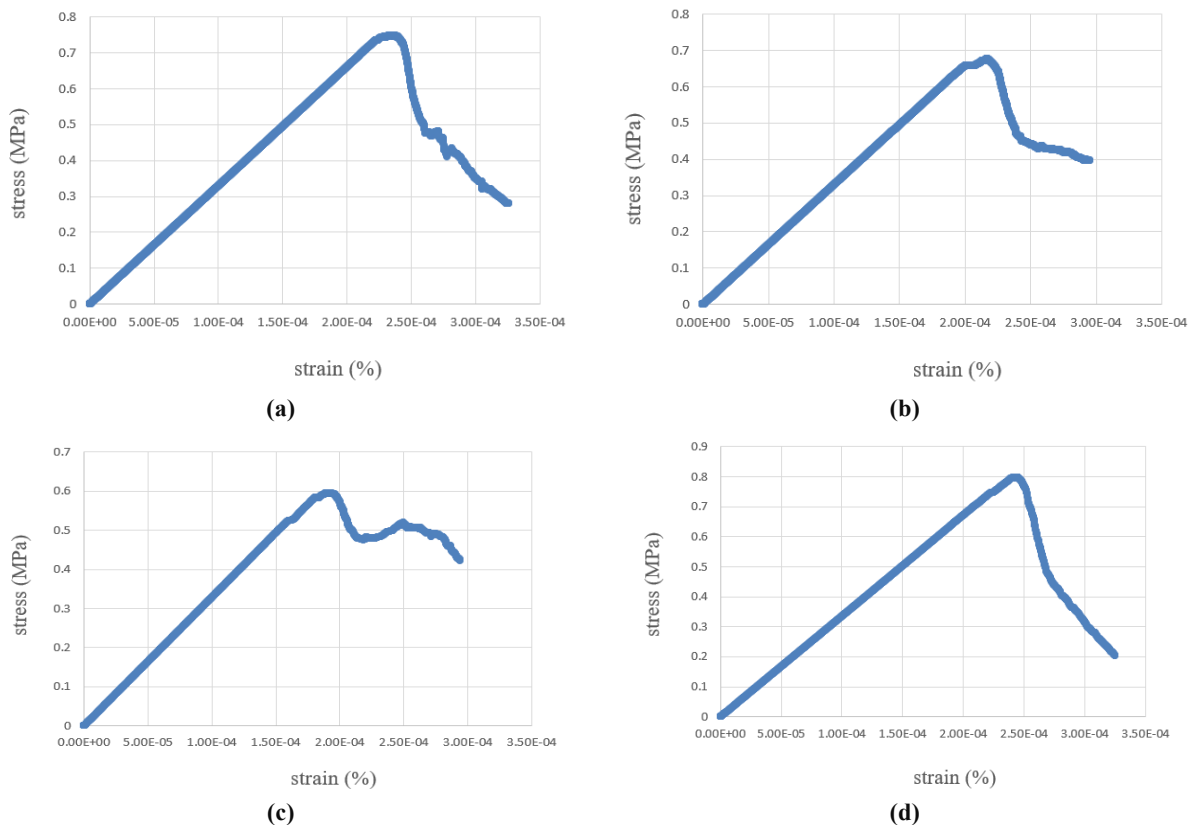


Figure 16. Stress versus strain for four models with different large joint angles of a) 0, b) 30, c) 60, and d) 90.

b) Large joint length was 4 cm and small joint length was 2 cm

The failure and fracture mechanism of the modeled specimens with two T-shape non-persistent joints are shown in Figure 17. In this figure, the induced tensile and shear cracks are represented with black and red colors, respectively. Figure 18 shows the stress-strain curves and the mechanical behavior of the four simulated models with the 0, 30, 60, and 90

degrees joint inclination angles (for the large joint). Figure 17a shows the failure mechanism and the propagation of two induced tensile cracks originating from the upper and lower tips of the large horizontal joint in the modeled specimen. These cracks and another tensile crack originating from the middle part of the large joint are extended toward the specimens' boundaries preferably in the direction of the applied load. Figures 17b and 17c show the mechanism of

failure and fracture patterns for the models with the large joints of 30 and 60 degrees inclination angles, respectively. Again, the tensile cracks are originating from the upper and lower crack tips of the large crack and the middle parts of the small joints, and extend toward the specimens boundaries parallel to the loading direction. The

stress-strain curves representing the mechanical behavior of the modeled samples are shown in Figure 18. The minimum value of the strain at the failure point of the models is for the large joint of 60 degrees inclination (concerning the loading direction).

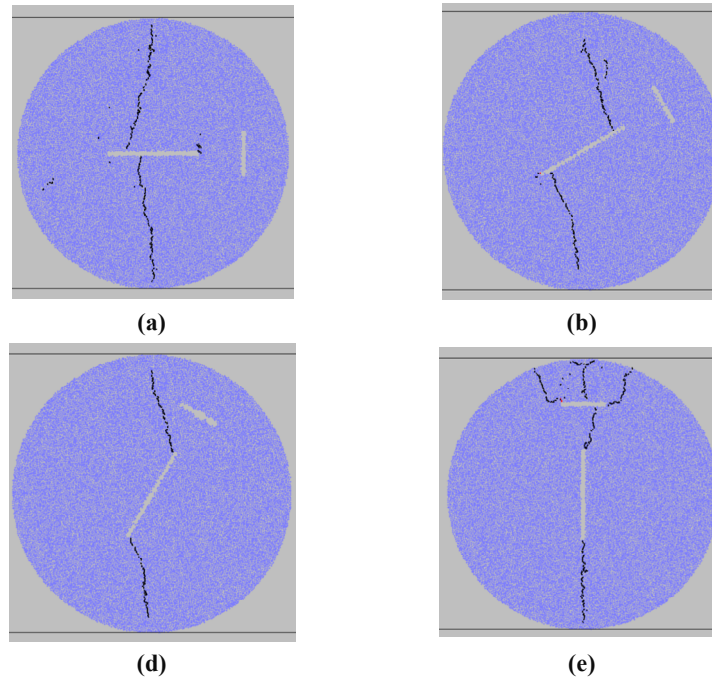


Figure 17. Failure pattern of specimens containing three non-persistent joint with large joint angle of a) 0, b) 30, c) 60, d) 90, e) 120, and f) 150.

c) Large joint length was 6 cm and small joint length was 3 cm

Figure 19 shows the fracture and failure mechanism of the modeled specimens with large and small joints of 6 and 3 cm in length, respectively. The red and black colors show the induced shear and tensile cracks in the modeled samples. On the other hand, Figure 20 shows the stress-strain curves representing the mechanical behavior of the modeled specimens in which the inclination angle of the large joint changes as 0, 30, 60, and 90 degrees.

Figure 19a shows the fracture patterns in the modeled sample for the case of a horizontal large joint (with a 0-degree inclination angle). In this case, two tensile cracks originated from the large crack tips, and also one tensile crack initiated from the middle part of the crack. These cracks may extend to the boundaries of the specimen

parallel to the loading direction. Figure 19b shows the fracture patterns for a modeled sample with a large joint of 30 degrees inclination angle related to the loading direction. In this case, one tensile crack is initiated from the upper tip, one originated from the lower tip of the large crack and another one is started from the middle part of the small crack. These cracks may extend toward the specimen's boundaries in the direction of the applied load. For the case of specimens with large cracks of 60 and 90 degrees inclination, the tensile cracks may induce at the upper and lower tips and also at the middle part of the large crack in the models, as shown in Figures 19c and 19d, respectively. These cracks also extend toward the boundaries of the specimen in the loading directions. The stress-strain curves of these modeled specimens are shown in Figure 20. The minimum value of the strain at failure is for the case of a large joint with 60 degrees inclination.

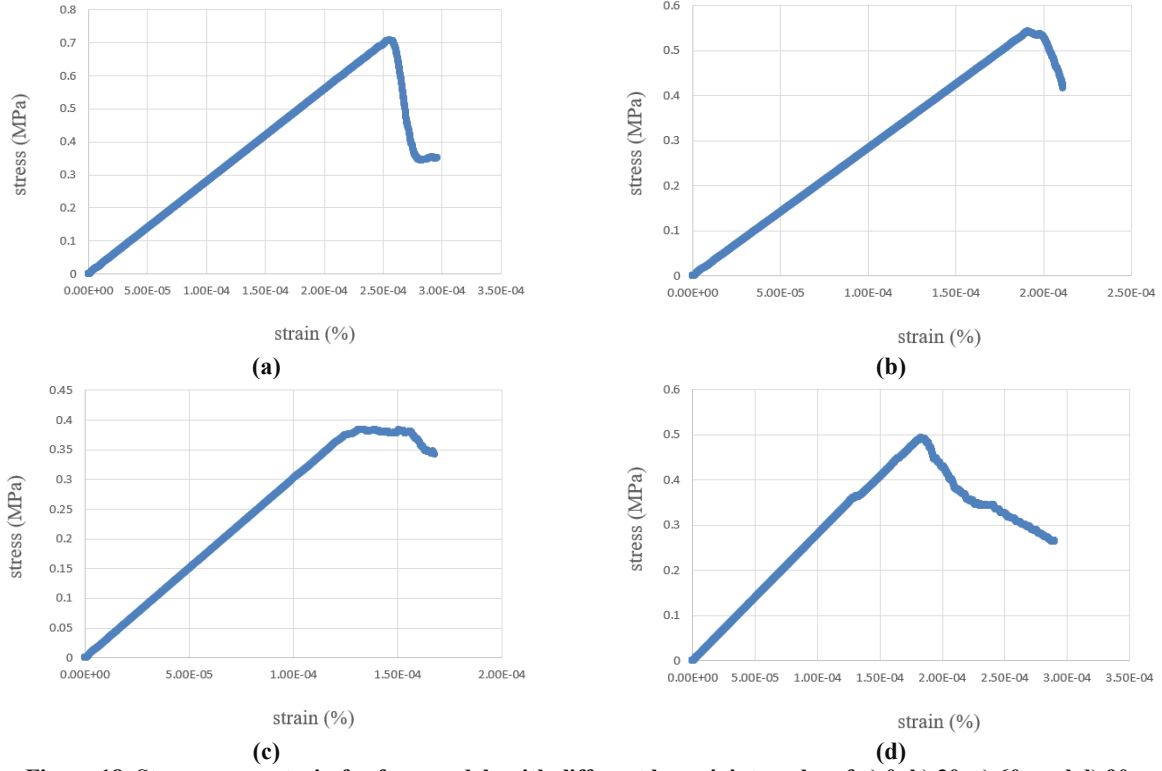


Figure 18. Stress versus strain for four models with different large joint angles of a) 0, b) 30, c) 60, and d) 90.

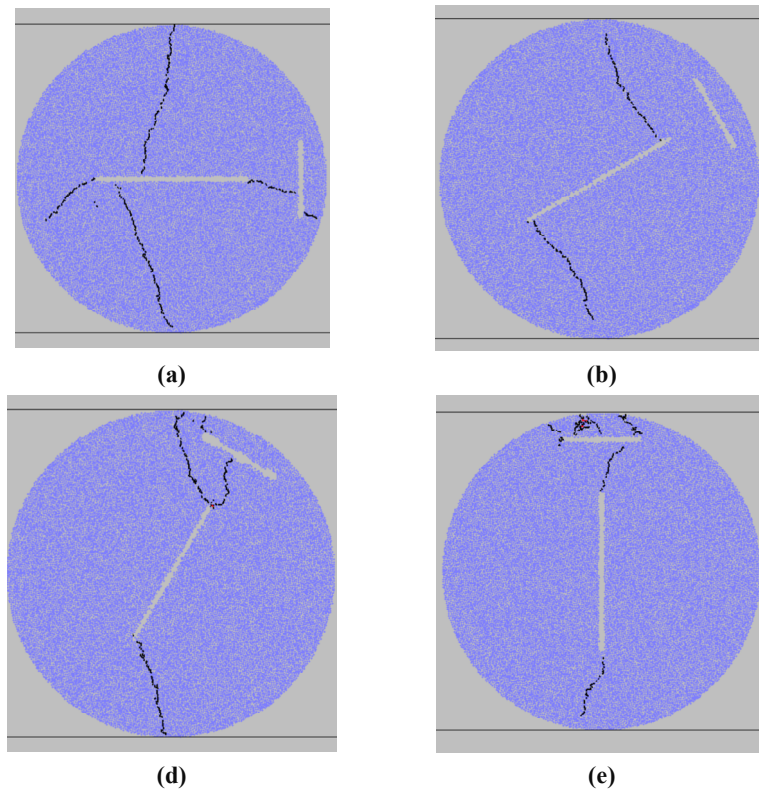


Figure 19. Failure pattern of specimens containing two non-persistent joint with large joint angle of a) 0, b) 30, c) 60, d) 90, e) 120, and f) 150

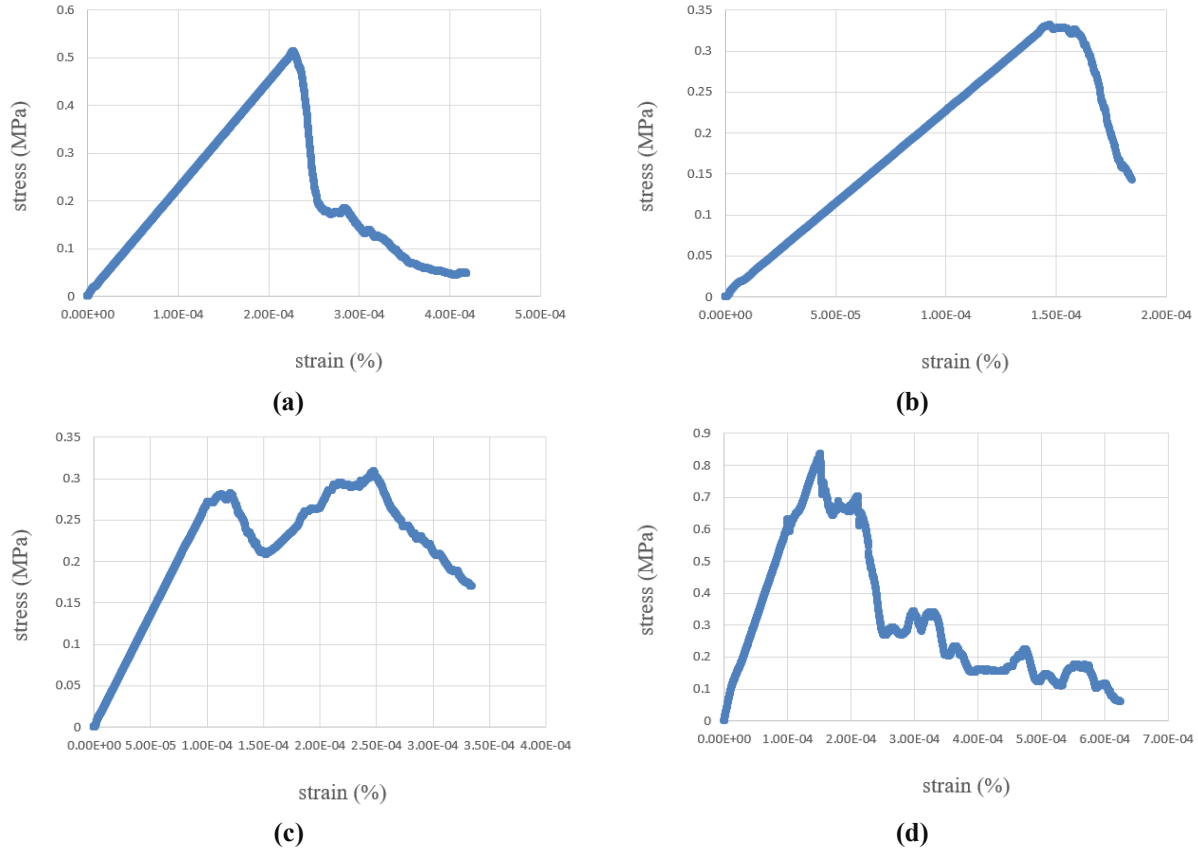


Figure 20. Stress versus strain for four models with different large joint angles of a) 0, b) 30, c) 60, and d) 90.

By comparison between Figures 21, 22, and 23, it could be concluded that the strain at failure point decrease by increasing the joint length.

By comparison between Figures 7-9 and Figures 15, 17 and 19, it can be concluded that failure pattern is similar in both of the experimental test and numerical simulation.

4.5. Effect of joint angle on strength of samples

Figure 21 shows the effect of joint angle and joint length on the strength of models. This figure was presented for three joint lengths. When the large joint angle was 60, the strength of the samples had a minimum value. When the large joint angle was 90, the strength of the samples had a maximum value. Also the strength of samples decreases by increasing the joint length.

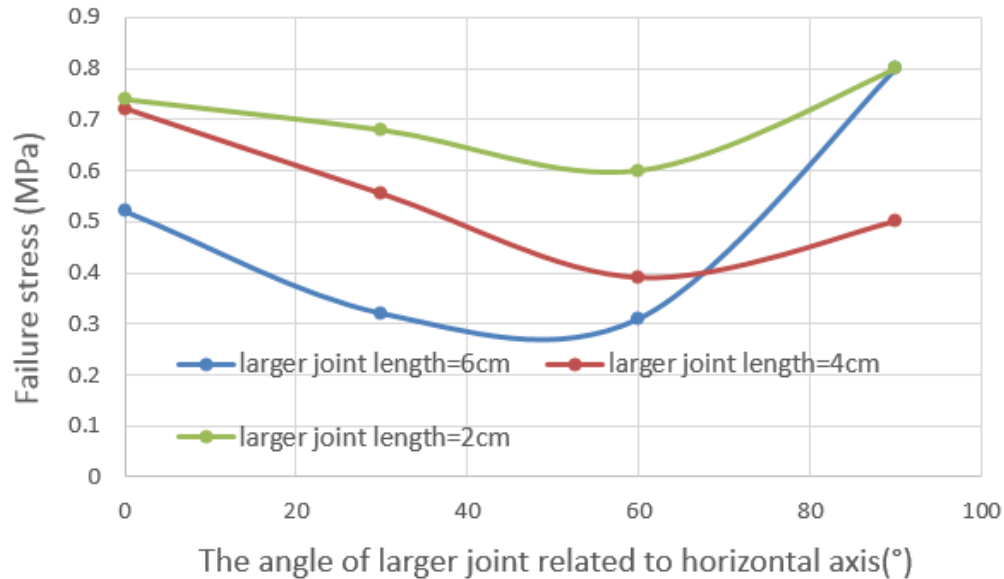


Figure 21. Effect of joint angle on strength of models.

By comparison between Figure 10 and Figure 21, it can be concluded that failure strength is nearly similar in both of the experimental test and numerical simulation.

5. Conclusions

The influence of cracks' geometrical parameters such as lengths and inclination angles of the cracked geo-material samples on the mechanical characteristics, strength, and fracture mechanism of the prepared specimens with non-persistence joints were studied in this research work. The effects of joints' bridge areas in the Brazilian tensile strengths of the concrete discs with 100 mm in diameter and 40 mm in thickness were studied using both the experimental tests and particle flow code in two dimensions (PFC2D). 12 experimental tests and 18 numerical models were used to completely consider the various scenarios and conditions of different problems in this work. The following main conclusions could be gained:

- For the flat lengthy joints with 0-degree inclination angles, two wing cracks are produced and propagate toward the boundary of the specimen parallel to the loading direction. For the lengthy cracks, one crack may start its propagation from the middle part of the original joint.

- When the large cracks are inclined at about 30 degrees concerning the loading direction, wing cracks initiate from the upper tips of the large cracks and continue their growth toward the boundary of the specimen. They may also coalesce with the other adjacent joints or cracks. For large joints with inclination angles of 60 and 90 degrees, the wing cracks initiate from the upper tip of the large joint and grow parallel to the loading axis till coalescence with the small joint.
- For lengthy joints, one tensile crack initiates from the wall of the small joint and propagates parallel to the loading axis till reaches the specimen's boundary. Some tensile cracks may also initiate from the lower tips of the larger joints and extend in the direction of loading till meet the boundaries of the specimens. The failure pattern was unchangeable by increasing the T shape joint length.
- The stress versus strain shows that this curve has a linear trend for different models till the failure occurs. The strain at the failure point has a minimum value when the large joint angle was 60. When the large joint angle was 60, the strength of the samples had a minimum value. When the large joint angle was 90, the strength of the samples had a maximum value.
- The strength of samples decreases by increasing the joint length. Strain at the failure point decrease by increasing the joint length.
- Failure strength and failure pattern are similar in both experimental tests and numerical simulation.

References

- [1]. Wong, R.H.C. and Chau, K.T. (1998). Crack coalescence in a rock-like material containing two cracks. *Int J Rock Mech Min Sci.* 35 (2):147–164.
- [2]. Ghazvinian, A., Sarfarazi, V., Schubert, W., and Blumel, M. (2012). A study of the failure mechanism of planar non-persistent open joints using PFC2D. *Rock Mech. Rock Eng.* 45 (5): 677-693.
- [3]. Fujii, Y. and Ishijima, Y. (2005). Consideration of fracture growth from an inclined slit and inclined initial fracture at the surface of rock and mortar in compression. *Int J Rock Mech Min Sci.* 41 (6):1035–1041.
- [4]. Sarfarazi, V., Haeri, H., Shemirani, A.B., Zhu, Z. (2017) Shear Behavior of Non-Persistent Joint Under High Normal Load. *Strength Mater.* 49: 320–334.
- [5]. Yang, S.Q. and Jing, H.W. (2011). Strength failure and crack coalescence behavior of brittle sandstone samples containing a single fissure under uniaxial compression. *Int J Fract.*,168:227–250.
- [6]. Yang, S.Q., Liu, X.R., and Jing, H.W. (2013). Experimental investigation on fracture coalescence behavior of red sandstone containing two unparallel fissures under uniaxial compression. *Int J Rock Mech Min Sci.*, 63:82–92.
- [7]. Yin, P., Wong R.H.C, and Chau K.T. (2014). Coalescence of two parallel pre-existing surface cracks in granite. *Int J Rock Mech Min Sci.* 68 (6):66–84.
- [8]. Zhuang, X., Chun, J., and Zhu, H. (2014). A comparative study on unfilled and filled crack propagation for rock-like brittle material. *Theor Appl Fract Mech.* 72 (1):110.
- [9]. Sarfarazi, V. and Haeri, H. (2016). Effect of number and configuration of bridges on shear properties of sliding surface”, *J. Min. Sci.* 52 (2):245-257.
- [10]. Yang, S.Q., Huang, Y.H., and Ranjith, P.G. (2018). Failure mechanical and acoustic behavior of brine saturated-sandstone containing two pre-existing flaws under different confining pressures. *Eng Fract Mech.*; 193:108–121.
- [11]. Şeref, D. (2019), Non-linear behavior of fiber reinforced cracked composite beams. *Steel and Composite Structures, An Int'l Journal.* 30 (4): 232-246.
- [12]. Bilge, H., Doruk, E., and Fehim, F. (2019). Effect of fatigue crack propagation on natural frequencies of system in AISI 4140 Steel. *Steel and Composite Structures, An Int'l Journal.* 32 (3): 145-161.
- [13]. Memarzadeh, P. and Mousavian, M. (2020). Effect of crack location on buckling analysis and SIF of cracked plates under tension. *Steel and Composite Structures, An Int'l Journal.* 35 (2): 213-222.
- [14]. Xu, C. and Zhang, B. (2020). Cracking and bending strength evaluations of steel-concrete double composite girder under negative bending action. *Steel and Composite Structures, An Int'l Journal.*, 35(3): 232-245.
- [15]. Yang, S.Q., Huang, Y.H., Jing, H.W., and Liu, X.R. (2014). Discrete element modeling on fracture coalescence behavior of red sandstone containing two unparallel fissures under uniaxial compression. *Eng Geol.* 178 (6):28–48.
- [16]. Lee, H and Jeon, S. (2011). An experimental and numerical study of fracture coalescence in pre-cracked specimens under uniaxial compression. *Int J Solids Struct.* 48 (6):979–999.
- [17]. Lee, J.S., Sagong, M., Yoo, J., and You, K. (2012). Analytical modeling and experimental verification of a tunnel with joint sets. *Int J Rock Mech Min Sci.* 50 (2): 56–64.
- [18]. Haeri, H., Sarfarazi, V., and Lazemi, H.A. (2016). Experimental study of shear behavior of planar non-persistent joint. *Comput. Concrete.* 17 (5): 639-653.
- [19]. Abdollahi M. S., Najafi M., Yarahmadi Bafghi A.R., and Fatehi Marji M. (2019). A 3D numerical model to determine suitable reinforcement strategies for passing TBM through a fault zone, a case study: Safaroud water transmission tunnel, Iran, *Tunneling and Underground Space Technology* 88, 186-199.
- [20]. Gil, D.M. and Golewski, G.L. (2018). Potential of siliceous fly ash and silica fume as a substitute of binder in cementitious concrete, *E3S Web Conf.*, 49, 00030.
- [21]. Zhang, P., Han, S., Golewski, G.L., and Wang, X. (2020). Nanoparticle-reinforced building materials with applications in civil engineering. *Adv. Mech. Eng.*, 12, 1–4.
- [22]. Golewski, G.L. (2021). On the special construction and materials conditions reducing the negative impact of vibrations on concrete structures, *Materials Today: Proceedings*, 66-77.
- [23]. Golewski, G.L. (2021). Green concrete based on quaternary binders with significant reduced of CO₂ emissions, *Energies* 14, 4558.

- [24]. Golewski, G.L. (2022). Strength and microstructure of composites with cement matrixes modified by fly ash and active seeds of CSH phase, *Structural Engineering and Mechanics*. 82 (4): 543-556.
- [25]. Yaylacı, M. (2022). Simulate of edge and an internal crack problem and estimation of stress intensity factor through finite element method. *Advances in Nano-research*. 12 (4): 405-414.
- [26]. Öner, E., Şengül Şabano, B., Uzun Yaylacı, E., Adıyaman, G., Yaylacı, M., and Birinci, A. (2022). On the plane receding contact between two functionally graded layers using computational, finite element and artificial neural network methods. *Journal of Applied Mathematics and Mechanics*, <https://doi.org/10.1002/zamm.202100287>
- [27]. Uzun, Yaylacı, E., Öner, E., Yaylacı, M., Özdemir, M.E., Abushattal, A., and Birinci, A. (2022). Application of artificial neural networks in the analysis of the continuous contact problem. *Structural Engineering and Mechanics*. 84 (1): 35-48.
- [28]. Yaylacı, M., Abanoz, M., Uzun Yaylacı, E., Ölmez, H., Sekban, M.D., and Birinci, A. (2022). The contact problem of the functionally graded layer resting on rigid foundation pressed via rigid punch. *Steel and Composite Structures*. 43 (5):661-672.
- [29]. Yaylacı, M., Şengül Şabano, B., Özdemir, M.E., Birinci, A. (2022). Solving the contact problem of functionally graded layers resting on a homogeneous half-plane and pressed with a uniformly distributed load by analytical and numerical methods, *Structural Engineering and Mechanics*. 82 (3): 401-416.
- [30]. Wang, Y., Zhou, X., Xu, X. (2016). Numerical simulation of propagation and coalescence of flaws in rock materials under compressive loads using the extended non-ordinary statebased peridynamics, *Eng Fract Mech.*,163:248–273.
- [31]. Prudencio M. and Jan M.V.S. (2007). Strength and failure modes of rock mass models with nonpersistent joints, *Int J Rock Mech Min Sci*. 44 (6):890–902.
- [32]. Chen, X., Liao, Z.H., and Peng, X. (2012). Deformability characteristics of jointed rock masses under uniaxial compression. *Int J Min Sci Technol*. 22 (2):213–221.
- [33]. Chen, X., Liao, Z.H., and Peng, X. (2013). Cracking process of rock mass models under uniaxial compression, *J Cent South Univ*. 20 (6):1661–1678.
- [34]. Cheng, C., Chen, X., and Zhang, S. (2016). Multi-peak deformation behavior of jointed rock mass under uniaxial compression: insight from particle flow modeling, *Eng Geol.*, 213:25–45.
- [35]. Haeri, H. (2015), Experimental crack analyses of concrete-like CSCBD specimens using a higher order DDM, *Comput. Concrete*. 16 (6):881- 896.
- [36]. Price, N.J. (1996). *Fault and Joint Development in Brittle and Semi-brittle Rock*. Oxford: Pergamon Press.
- [37]. Tang, C.A., Lin, P., Wong, R.H.C., and Chau, K.T. (2001). Analysis of crack coalescence in rock-like materials containing three flaws-part II: numerical approach, *Int JRock MechMin Sci*. 38 (7): 925–939.
- [38]. Wan, S.Y., Sloan, S.W., Sheng, D.C., Yang, S.Q., and Tang, C.A. (2014). Numerical study of failure behavior of pre-cracked rock specimens under conventional triaxial compression, *Int J Solids Struct*. 51 (5):1132–1148.
- [39]. Fatehi Marji F. (1997). Modelling of cracks in rock fragmentation with a higher order displacement discontinuity method, PhD Thesis in Mining Engineering (Rock Mechanics), METU, Ankara, Turkey.
- [40]. Xie, Y., Cao P., Liu, J., and Dong, L. (2016). Influence of crack surface friction on crack initiation and propagation: a numerical investigation based on extended finite element method, *Comput Geotech.*,74:1–14.
- [41]. Pu, C.Z. and Cao, P. (2012). failure characteristics and its influencing factors of rock-like material with multi-fissures under uniaxial compression, *Appl Mech Mater*. 711 (1):129–132.
- [42]. Sagong, M. and Bobet, A. (2002). Coalescence of multiple flaws in a rock-model material in uniaxial compression, *Int J Rock Mech Min Sci*. 39 (2):229–241.
- [43]. Sagong, M., Park, D., Yoo, J., and Lee, J.S. (2011). Experimental and numerical analyses of an opening in a jointed rock mass under biaxial compression, *Int J Rock Mech Min Sci*. 48 (7):1055–1067.
- [44]. Wang, Y., Zhou, X., and Shou, Y. (2017). The modeling of crack propagation and coalescence in rocks under uniaxial compression using the novel conjugated bond-based peridynamics, *Int J Mech Sci.*, 128:614–643.
- [45]. Potyondy D.O. and Cundall P. A. (2004). A bonded-particle model for rock, *International Journal of Rock Mechanics and Mining Sciences*. 41 (8):1329–1364.

شبیه سازی PFC تست مقاومت کششی برزلی در نمونه‌های ژئومواد با درزه‌های ناممتد T شکل

وهاب سرفرازی^۱، هادی حائری^۲، فرشته باقری^۱، عرفان زرین قلم^۱، و محمد فاتحی مرچی^{۳*}

۱-بخش مهندسی معدن، دانشگاه صنعتی همدان، همدان، ایران

۲-بخش مهندسی معدن، مجتمع آموزش عالی زرنند، زرنند، ایران

۳-بخش مهندسی معدن، دانشکده معدن و متالورژی، دانشگاه یزد، یزد، ایران

ارسال ۲۰۲۲/۱۱/۱۴، پذیرش ۲۰۲۲/۱۲/۰۴

* نویسنده مسئول مکاتبات: mohammad.fatehi@gmail.com

چکیده:

مقاومت کششی مواد ژئومتری مانند سنگ، سرامیک، بتن، گچ و ملات بر اساس آزمایش مقاومت کششی مستقیم و غیر مستقیم به دست می‌آید. در این کار تحقیقاتی، از آزمون‌های مقاومت کششی برزلی برای بررسی اثرات طول و زاویه شیب درزه‌های ناممتد T شکل بر رفتارهای مکانیکی و کششی نمونه‌های ژئومتریال تهیه شده از بتن استفاده می‌شود. این نمونه‌ها دارای ضخامت ۴۰ میلی‌متر و قطر ۱۰۰ میلی‌متر هستند و در آزمایشگاه تهیه می‌شوند. در هر نمونه دیسک برزلی دو درزه ناممتد T شکل ایجاد می‌شود. نمونه‌های دیسک برزلی با درزه‌های ناممتد T شکل به صورت تجربی در آزمایشگاه تحت فشار محوری آزمایش می‌شوند. سپس این آزمایش‌ها در کد دوبعدی جریان ذرات (PFC2D) با در نظر گرفتن طول‌های ترک (ناچ) مختلف ۴، ۳، ۲ و ۱ سانتی‌متر شبیه‌سازی می‌شوند. با این حال، زوایای شیب ناچ مختلف ۰، ۳۰، ۶۰، ۹۰، ۱۲۰ و ۱۵۰ درجه نیز در نظر گرفته شده است. در این کار تحقیقاتی، ۱۲ نمونه با پیکربندی‌های مختلف برای آزمایش‌های تجربی ارائه شده است و ۱۸ مدل PFC2D برای مطالعات عددی این آزمایش‌ها ساخته شده است. نرخ بارگذاری ۰/۰۱۶ میلی‌متر بر ثانیه است. نتایج به دست آمده از این آزمایش‌ها و مدل‌های شبیه‌سازی شده آن‌ها با هم مقایسه می‌شوند و نتیجه‌گیری می‌شود که رفتار مکانیکی و فرآیند شکست این نمونه‌های ژئومتریال عمدتاً توسط زوایای شیب و طول درزه‌های ناممتد T شکل ارائه شده در نمونه‌ها کنترل می‌شود. مکانیسم شکست و رفتار شکست نمونه‌ها توسط ناپیوستگی‌ها و تعداد ترک‌های ناشی از افزایش زوایای شیب درزه و طول درزه‌ها کنترل می‌شود. برای درزه‌های بزرگتر زمانی که زاویه شیب درزه ناممتد T شکل حدود ۶۰ درجه است، مقاومت کششی حداقل است اما از آنجایی که تا ۹۰ درجه بسته است، مقاومت فشاری حداکثر است. با این حال، افزایش طول شکاف، مقاومت کششی کلی نمونه‌ها را افزایش می‌دهد. مقاومت نمونه‌ها با افزایش طول درزه کاهش می‌یابد. کرنش در نقطه شکست با افزایش طول درزه کاهش می‌یابد. همچنین مشاهده می‌شود که روند مقاومت و شکست دو مجموعه از نمونه‌ها و شبیه‌سازی‌های عددی مربوطه با هم سازگاری دارند.

کلمات کلیدی: درزه ناممتد T شکل، زاویه درزه، طول درزه، PFC2D.